

# Investigating entropic dynamics of multiqubit cavity QED system

Miao Hui-hui\*

*Faculty of Computational Mathematics and Cybernetics,  
Lomonosov Moscow State University, Vorobyovy Gory 1, Moscow, 119991, Russia*

(Dated: May 27, 2024)

Entropic dynamics of a multiqubit cavity quantum electrodynamics system is simulated and various aspects of entropy are explored. In the modified version of the Tavis–Cummings–Hubbard model, atoms are held in optical cavities through optical tweezers and can jump between different cavities through the tunneling effect. The interaction of atom with the cavity results in different electronic transitions and the creation and annihilation of corresponding types of photon. Electron spin and the Pauli exclusion principle are considered. Formation and break of covalent bond and creation and annihilation of phonon are also introduced into the model. The system is bipartite. The effect of all kinds of interactions on entropy is studied. And the von Neumann entropy of different subsystems is compared. The results show that the entropic dynamics can be controlled by selectively choosing system parameters, and the entropy values of different subsystems satisfy certain inequality relationships.

Keywords: entropic dynamics, finite-dimensional QED, artificial atom, covalent bond, phonon.

## I. INTRODUCTION

The idea of entropy was initially introduced to thermodynamics in 1865 by Clausius [1]. Subsequently, Boltzmann established the relationship between entropy and the system’s microscopic characteristics and gave it statistical significance. Entropy is a measure of the degree of disorder in a microscopic system used in statistical physics. In 1929, Szilard provided an explanation of the connection between information and entropy. Entropy is used as a measure of information in information theory. Later, von Neumann expanded classical entropy to the quantum domain [2]. And entropy is used to investigate entanglement in the interaction between light and matter [3–8]. Shannon then developed information theory based on Boltzmann’s classical entropy [9]. On the other hand, the phenomena of quantum entanglement has garnered a lot of attention with the advancement of quantum mechanics and the founding of quantum information science. Einstein and other scientists were the first to observe the phenomena of quantum entanglement [10, 11]. Quantum entanglement is currently widely applied in quantum communications and quantum information processing. Measuring the quantum entanglement between two-body pure state systems is one of the key functions of quantum entropy. To this day, the quantum entropy can be found using a variety of quantifiers, including information entropy [12–14], conditional entropy [15, 16], relative entropy [17], compressed entropy [18, 19], differential entropy [20], etc [21–29]. In recent years, the wide application of quantum entropy theory in the fields of quantum optics and quantum information has attracted great attention. It is the theoretical basis and powerful tool for understanding hot topics of quantum mechanics and quantum informatics [30–35].

A key contribution of this research is the model of quantum electrodynamics (QED), which offers a unique scientific framework for studying the interaction between matter and light. Fields of cavities in this paradigm are coupled to impurity two- or multi-level structures, usually called atoms. The Jaynes–Cummings model (JCM) [36] and Tavis–Cummings model (TCM) [37] and their generalizations — Jaynes–Cummings–Hubbard model (JCHM) and Tavis–Cummings–Hubbard model (TCHM) [38], which are usually easier to achieve in experiment, are the most researched cavity QED models. Recent years have seen a significant amount of study in the field of cavity QED models [39–49]. There are some applications for entropy in quantum computations. Nevertheless, prior research has primarily focused on entropic dynamics in simple cavity QED systems, with a rare exception of more complicated systems. Consequently, it is imperative to examine entropic dynamics in complicated systems.

Since von Neumann entropy has so many uses and special characteristics in quantum mechanics and quantum informatics, we employ it to calculate quantum entropy and study its properties in this paper. We simulate and investigate von Neumann entropy in the complicated bipartite system, based on the modified version of the TCHM, consists of two subsystems.

This paper is organized as follows. After introducing the target model — the neutral hydrogen molecule association-dissociation model with covalent bond and phonon in Sec. II, we introduce numerical method in Sec. III A and definitions of von Neumann entropy in Sec. III B. We present the effect of interactions on entropy and comparison of entropy of different subsystems in Secs. IV A and IV B, respectively. Some brief comments on our results and extension to future work in Sec. V close out the paper. Some technical details are included in Appendices A, B and C. List of all abbreviations and notations used in this paper is put in Appx. D.

---

\* Email address: hhmiao@cs.msu.ru

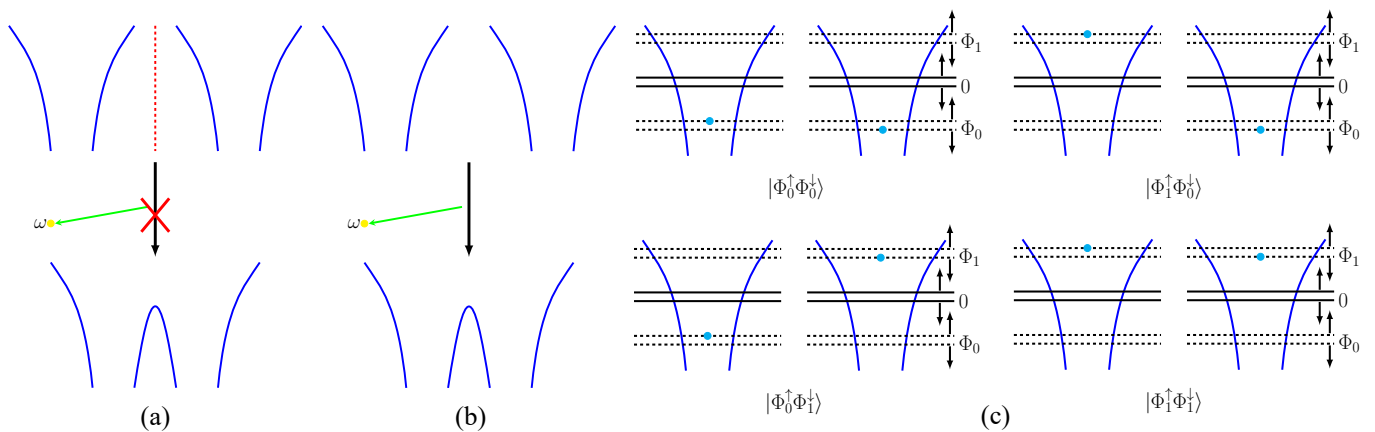


FIG. 1. (online color) *The model with covalent bond and phonon.* When atoms are in distinct cavities depicted in panel (a), hybridization of atomic orbitals is prohibited; however, when atoms are in the same cavity depicted in panel (b), hybridization of atomic orbitals is allowed. As atomic orbitals hybridize, a covalent bond is formed and a phonon is released; conversely, when a covalent bond is broken, a phonon is absorbed. In panel (c), initial state of entire system, denoted by  $|\Psi_{initial}\rangle$ , is  $|0_1^\uparrow\rangle_e|0_2^\downarrow\rangle_e$ . According to Eqs. (1) and (2),  $|\Psi_{initial}\rangle$  can be decomposed into the sum of four states  $|\Phi_0^\uparrow\Phi_0^\downarrow\rangle$ ,  $|\Phi_1^\uparrow\Phi_0^\downarrow\rangle$ ,  $|\Phi_0^\uparrow\Phi_1^\downarrow\rangle$  and  $|\Phi_1^\uparrow\Phi_1^\downarrow\rangle$  (see Eqs. (12) and (13)). In the panels, the blue and yellow dots, respectively, stand for electrons and photons. The vertical red dashed line in panel (a) indicates a significant distance between the cavities.

## II. THE NEUTRAL HYDROGEN MOLECULE ASSOCIATION-DISSOCIATION MODEL WITH COVALENT BOND AND PHONON

The association-dissociation model of the neutral hydrogen molecule, studied in detail in our previous work on quantum evolution [46, 47], is modified from the TCHM. In this paper, we directly quote the model called the neutral hydrogen molecule association-dissociation model with covalent bond and phonon from [46] and study the entropy dynamics and its various aspects in the non-dissipative case, that is to say, in a closed quantum system. So in this paper we do not use the quantum master equation (QME) — Lindbladian.

There are two hydrogen atoms in the model, which form hydrogen bond through orbital hybridization and release a phonon. On the contrary, when the hydrogen bond is broken, phonon need to be absorbed. Both the association and the dissociation reactions can be interpreted by this target model. Each energy level in the molecular-atomic system — both atomic and molecular — is divided into two levels, spin up and spin down, denoted by the signs  $\uparrow$  and  $\downarrow$ , respectively. There will now be twice as many levels, and the Pauli exclusion principle [50] dictates that each level can only contain one electron. Electron spin flips are temporarily ignored. The excited states of the electron with the spins for the first nucleus are indicated by  $|0_1^\uparrow\rangle_e$  and  $|0_1^\downarrow\rangle_e$ . Usually simply written as  $|0_1\rangle_e$ , which can denote both  $|0_1^\uparrow\rangle_e$  and  $|0_1^\downarrow\rangle_e$ . For the second nucleus —  $|0_2\rangle_e$ , which can denote both  $|0_2^\uparrow\rangle_e$  and  $|0_2^\downarrow\rangle_e$ . Hybridization is impossible when two atoms are in different cavities (see Fig. 1 (a)). Only when two atoms are in the same cavity, orbital hybridization is possible (see Fig. 1 (b)).

Hybrid molecular states of the electron are denoted by

$$|\Phi_1\rangle_e = \frac{1}{\sqrt{2}} (|0_1\rangle_e - |0_2\rangle_e) \quad (1a)$$

$$|\Phi_0\rangle_e = \frac{1}{\sqrt{2}} (|0_1\rangle_e + |0_2\rangle_e) \quad (1b)$$

where  $|\Phi_1\rangle_e$  is molecular excited state,  $|\Phi_0\rangle_e$  is molecular ground state. On the contrary, we can get the atomic state after orbital de-hybridization

$$|0_1\rangle_e = \frac{1}{\sqrt{2}} (|\Phi_0\rangle_e + |\Phi_1\rangle_e) \quad (2a)$$

$$|0_2\rangle_e = \frac{1}{\sqrt{2}} (|\Phi_0\rangle_e - |\Phi_1\rangle_e) \quad (2b)$$

The Hilbert space of quantum states of the entire system, having the following form

$$|\Psi\rangle_{\mathcal{C}} = |p_1\rangle_{\Omega^\uparrow}|p_2\rangle_{\Omega^\downarrow}|m\rangle_\omega|l_1\rangle_{\Phi_1^\uparrow}|l_2\rangle_{\Phi_1^\downarrow}|L\rangle_{cb}|k\rangle_n \quad (3)$$

where  $p_1$ ,  $p_2$  are the numbers of molecular photons with modes  $\Omega^\uparrow$ ,  $\Omega^\downarrow$ , respectively;  $m$  is the number of phonons with mode  $\omega$ .  $l_1$ ,  $l_2$  describe orbital state:  $l_1 = 1$  — electron with spin  $\uparrow$  in excited orbital  $\Phi_1^\uparrow$ ,  $l_1 = 0$  — electron with spin  $\uparrow$  in ground orbital  $\Phi_0^\uparrow$ ;  $l_2 = 1$  — electron with spin  $\downarrow$  in excited orbital  $\Phi_1^\downarrow$ ,  $l_2 = 0$  — electron with spin  $\downarrow$  in ground orbital  $\Phi_0^\downarrow$ . The states of the covalent bond are denoted by  $|L\rangle_{cb}$ :  $L = 0$  — covalent bond formation,  $L = 1$  — covalent bond breaking. The states of the nuclei are denoted by  $|k\rangle_n$ :  $k = 0$  — state of nuclei, gathering together in one cavity,  $k = 1$  — state of nuclei, scattering in different cavities.

Hamiltonian of this new model with consideration of rotation wave approximation (RWA, see Appx. A) has following form

$$\begin{aligned}
H = & \hbar\Omega^\dagger a_{\Omega^\dagger}^\dagger a_{\Omega^\dagger} + \hbar\Omega^\downarrow a_{\Omega^\downarrow}^\dagger a_{\Omega^\downarrow} + \hbar\omega a_\omega^\dagger a_\omega \\
& + \hbar\Omega^\dagger \sigma_{\Omega^\dagger}^\dagger \sigma_{\Omega^\dagger} + \hbar\Omega^\downarrow \sigma_{\Omega^\downarrow}^\dagger \sigma_{\Omega^\downarrow} + \hbar\omega \sigma_\omega^\dagger \sigma_\omega \\
& + g_{\Omega^\dagger} \left( a_{\Omega^\dagger}^\dagger \sigma_{\Omega^\dagger} + a_{\Omega^\dagger} \sigma_{\Omega^\dagger}^\dagger \right) \sigma_\omega \sigma_\omega^\dagger \\
& + g_{\Omega^\downarrow} \left( a_{\Omega^\downarrow}^\dagger \sigma_{\Omega^\downarrow} + a_{\Omega^\downarrow} \sigma_{\Omega^\downarrow}^\dagger \right) \sigma_\omega \sigma_\omega^\dagger \\
& + g_\omega \left( a_\omega^\dagger \sigma_\omega + a_\omega \sigma_\omega^\dagger \right) \\
& + \zeta \left( \sigma_n^\dagger \sigma_n + \sigma_n \sigma_n^\dagger \right)
\end{aligned} \tag{4}$$

where  $\hbar = h/2\pi$  is the reduced Planck constant.  $g$  is the coupling strength between the photon or phonon (with annihilation and creation operators  $a$  and  $a^\dagger$ , respectively) and the electron in the molecule (with excitation and relaxation operators  $\sigma^\dagger$  and  $\sigma$ , respectively).  $g_{\Omega^\dagger}$  is the coupling strength for the photon mode  $\Omega^\dagger$ ,  $g_{\Omega^\downarrow}$  is the coupling strength for the photon mode  $\Omega^\downarrow$ ,  $g_\omega$  is the strength of formation or breaking of covalent bond,  $\zeta$  is the tunneling strength.  $\sigma_\omega \sigma_\omega^\dagger$  verifies that covalent bond is formed. The matrix form of all operators are shown in Appx. B.

For this seven-qubit system of  $2^7$  states, in fact, only a small part of the states participate in the evolution, because we do not consider the dissipative process. In addition, the initial state and some conditions also limit the scale of the states participating in the evolution. We can generate these states through two steps:

- generating and numbering potential evolution states involved in the evolution in accordance with the initial state;
- establishing Hamiltonian with these states and potential interactions among them.

Using this technique, 17 states are obtained, which are shown in Tab. I and interactions between these states are shown in Fig. 2.

The photon annihilation and creation operators on an  $p_1$ -photon state with mode  $\Omega^\dagger$  are described as

$$\begin{aligned}
if \ p_1 > 0, & \begin{cases} a_{\Omega^\dagger} |p_1\rangle_{\Omega^\dagger} = \sqrt{p_1} |p_1 - 1\rangle_{\Omega^\dagger}, \\ a_{\Omega^\dagger}^\dagger |p_1\rangle_{\Omega^\dagger} = \sqrt{p_1 + 1} |p_1 + 1\rangle_{\Omega^\dagger}, \end{cases} \\
if \ p_1 = 0, & \begin{cases} a_{\Omega^\dagger} |0\rangle_{\Omega^\dagger} = 0, \\ a_{\Omega^\dagger}^\dagger |0\rangle_{\Omega^\dagger} = |1\rangle_{\Omega^\dagger}. \end{cases}
\end{aligned} \tag{5}$$

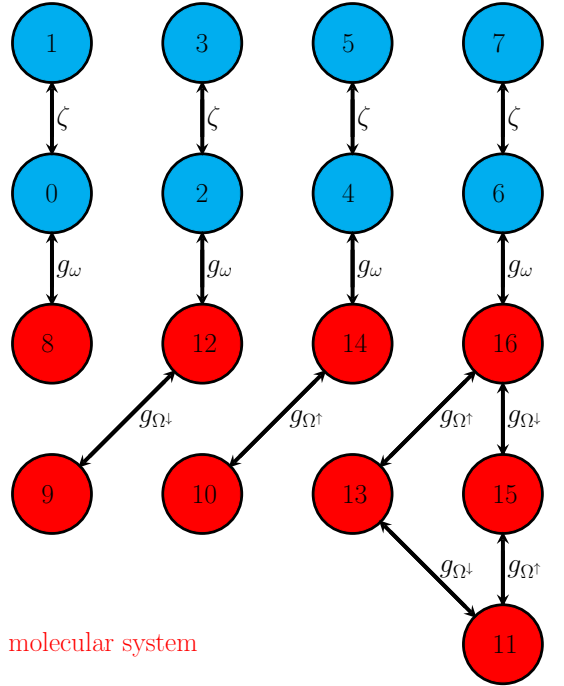
And their corresponding operators for electronic transitions,  $\sigma_{\Omega^\dagger}$ ,  $\sigma_{\Omega^\dagger}^\dagger$ , have following form

$$\begin{aligned}
\sigma_{\Omega^\dagger} |0\rangle_{\Phi^\dagger} &= 0, \\
\sigma_{\Omega^\dagger} |1\rangle_{\Phi^\dagger} &= |0\rangle_{\Phi^\dagger}, \\
\sigma_{\Omega^\dagger}^\dagger |0\rangle_{\Phi^\dagger} &= |1\rangle_{\Phi^\dagger}, \\
\sigma_{\Omega^\dagger}^\dagger |1\rangle_{\Phi^\dagger} &= 0.
\end{aligned} \tag{6}$$

State	Hilbert space	$ p_1\rangle p_2\rangle m\rangle l_1\rangle l_2\rangle L\rangle k\rangle$
Index		
0		$ 0\rangle 0\rangle 0\rangle 0\rangle 0\rangle 1\rangle 0\rangle$
1		$ 0\rangle 0\rangle 0\rangle 0\rangle 0\rangle 1\rangle 1\rangle$
2		$ 0\rangle 0\rangle 0\rangle 0\rangle 1\rangle 1\rangle 0\rangle$
3		$ 0\rangle 0\rangle 0\rangle 0\rangle 1\rangle 1\rangle 1\rangle$
4		$ 0\rangle 0\rangle 0\rangle 1\rangle 0\rangle 1\rangle 0\rangle$
5		$ 0\rangle 0\rangle 0\rangle 1\rangle 0\rangle 1\rangle 1\rangle$
6		$ 0\rangle 0\rangle 0\rangle 1\rangle 1\rangle 1\rangle 0\rangle$
7		$ 0\rangle 0\rangle 0\rangle 1\rangle 1\rangle 1\rangle 1\rangle$
8		$ 0\rangle 0\rangle 1\rangle 0\rangle 0\rangle 0\rangle 0\rangle$
9		$ 0\rangle 1\rangle 1\rangle 0\rangle 0\rangle 0\rangle 0\rangle$
10		$ 1\rangle 0\rangle 1\rangle 0\rangle 0\rangle 0\rangle 0\rangle$
11		$ 1\rangle 1\rangle 1\rangle 0\rangle 0\rangle 0\rangle 0\rangle$
12		$ 0\rangle 0\rangle 1\rangle 0\rangle 1\rangle 0\rangle 0\rangle$
13		$ 1\rangle 0\rangle 1\rangle 0\rangle 1\rangle 0\rangle 0\rangle$
14		$ 0\rangle 0\rangle 1\rangle 1\rangle 0\rangle 0\rangle 0\rangle$
15		$ 0\rangle 1\rangle 1\rangle 1\rangle 0\rangle 0\rangle 0\rangle$
16		$ 0\rangle 0\rangle 1\rangle 1\rangle 1\rangle 0\rangle 0\rangle$

TABLE I. Quantum states involving in evolution.

diatomic system



molecular system

FIG. 2. (online color) Interactions between quantum states. In this figure, four types of interactions are shown:  $g_{\Omega^\dagger}$ ,  $g_{\Omega^\downarrow}$ ,  $g_\omega$  and  $\zeta$ . The blue circles correspond to the break of the covalent bond, that is,  $|L\rangle_{cb} = |1\rangle_{cb}$ , which is a diatomic system. The red circles correspond to the formation of the covalent bond, that is,  $|L\rangle_{cb} = |0\rangle_{cb}$ , which is a molecular system. Initially, system state consists of four states  $|0\rangle$ ,  $|2\rangle$ ,  $|4\rangle$  and  $|6\rangle$ , corresponding to  $|\Phi_0^\dagger \Phi_0^\dagger\rangle$ ,  $|\Phi_0^\dagger \Phi_1^\dagger\rangle$ ,  $|\Phi_1^\dagger \Phi_0^\dagger\rangle$  and  $|\Phi_1^\dagger \Phi_1^\dagger\rangle$ , respectively, which are defined in Eq. (13).

The photon annihilation and creation operators on an  $p_2$ -photon state with mode  $\Omega^\downarrow$  are described as

$$\begin{aligned} \text{if } p_2 > 0, & \begin{cases} a_{\Omega^\downarrow} |p_2\rangle_{\Omega^\downarrow} = \sqrt{p_2} |p_2 - 1\rangle_{\Omega^\downarrow}, \\ a_{\Omega^\downarrow}^\dagger |p_2\rangle_{\Omega^\downarrow} = \sqrt{p_2 + 1} |p_2 + 1\rangle_{\Omega^\downarrow}, \end{cases} \\ \text{if } p_2 = 0, & \begin{cases} a_{\Omega^\downarrow} |0\rangle_{\Omega^\downarrow} = 0, \\ a_{\Omega^\downarrow}^\dagger |0\rangle_{\Omega^\downarrow} = |1\rangle_{\Omega^\downarrow}. \end{cases} \end{aligned} \quad (7)$$

And their corresponding operators for electronic transitions,  $\sigma_{\Omega^\downarrow}$ ,  $\sigma_{\Omega^\downarrow}^\dagger$ , have following form

$$\begin{aligned} \sigma_{\Omega^\downarrow} |0\rangle_{\Phi^\downarrow} &= 0, \\ \sigma_{\Omega^\downarrow} |1\rangle_{\Phi^\downarrow} &= |0\rangle_{\Phi^\downarrow}, \\ \sigma_{\Omega^\downarrow}^\dagger |0\rangle_{\Phi^\downarrow} &= |1\rangle_{\Phi^\downarrow}, \\ \sigma_{\Omega^\downarrow}^\dagger |1\rangle_{\Phi^\downarrow} &= 0. \end{aligned} \quad (8)$$

The phonon annihilation and creation operators on an  $m$ -phonon state with mode  $\omega$  are described as

$$\begin{aligned} \text{if } m > 0, & \begin{cases} a_\omega |m\rangle_\omega = \sqrt{m} |m - 1\rangle_\omega, \\ a_\omega^\dagger |m\rangle_\omega = \sqrt{m + 1} |m + 1\rangle_\omega, \end{cases} \\ \text{if } m = 0, & \begin{cases} a_\omega |0\rangle_\omega = 0, \\ a_\omega^\dagger |0\rangle_\omega = |1\rangle_\omega. \end{cases} \end{aligned} \quad (9)$$

And the operators for formation-breaking of covalent bond,  $\sigma_\omega$ ,  $\sigma_\omega^\dagger$ , have following form

$$\begin{aligned} \sigma_\omega |0\rangle_{cb} &= 0, \\ \sigma_\omega |1\rangle_{cb} &= |0\rangle_{cb}, \\ \sigma_\omega^\dagger |0\rangle_{cb} &= |1\rangle_{cb} \\ \sigma_\omega^\dagger |1\rangle_{cb} &= 0. \end{aligned} \quad (10)$$

The operators for tunneling process of nuclei,  $\sigma_n$ ,  $\sigma_n^\dagger$ , have following form

$$\begin{aligned} \sigma_n |0\rangle_n &= 0, \\ \sigma_n |1\rangle_n &= |0\rangle_n, \\ \sigma_n^\dagger |0\rangle_n &= |1\rangle_n \\ \sigma_n^\dagger |1\rangle_n &= 0. \end{aligned} \quad (11)$$

Initial state  $|\Psi_{initial}\rangle$  is shown in Fig. 1 (c), which can be decomposed into the sum of four states

$$|\Psi_{initial}\rangle = \frac{1}{2} \left( |\Phi_0^\uparrow \Phi_0^\downarrow\rangle + |\Phi_1^\uparrow \Phi_0^\downarrow\rangle - |\Phi_0^\uparrow \Phi_1^\downarrow\rangle - |\Phi_1^\uparrow \Phi_1^\downarrow\rangle \right) \quad (12)$$

where

$$|\Phi_0^\uparrow \Phi_0^\downarrow\rangle = |0\rangle_{\Omega^\uparrow} |0\rangle_{\Omega^\downarrow} |0\rangle_\omega |0\rangle_{\Phi_1^\uparrow} |0\rangle_{\Phi_1^\downarrow} |1\rangle_{cb} |1\rangle_n \quad (13a)$$

$$|\Phi_1^\uparrow \Phi_0^\downarrow\rangle = |0\rangle_{\Omega^\uparrow} |0\rangle_{\Omega^\downarrow} |0\rangle_\omega |1\rangle_{\Phi_1^\uparrow} |0\rangle_{\Phi_1^\downarrow} |1\rangle_{cb} |1\rangle_n \quad (13b)$$

$$|\Phi_0^\uparrow \Phi_1^\downarrow\rangle = |0\rangle_{\Omega^\uparrow} |0\rangle_{\Omega^\downarrow} |0\rangle_\omega |0\rangle_{\Phi_1^\uparrow} |1\rangle_{\Phi_1^\downarrow} |1\rangle_{cb} |1\rangle_n \quad (13c)$$

$$|\Phi_1^\uparrow \Phi_1^\downarrow\rangle = |0\rangle_{\Omega^\uparrow} |0\rangle_{\Omega^\downarrow} |0\rangle_\omega |1\rangle_{\Phi_1^\uparrow} |1\rangle_{\Phi_1^\downarrow} |1\rangle_{cb} |1\rangle_n \quad (13d)$$

### III. NUMERICAL METHOD

#### A. Precise time step integration method

We use the density matrix  $\rho$  to obtain the unitary evolution of the non-dissipative system. The solution  $\rho(t)$  may be approximately found as follows

$$\rho(t + dt) = \exp\left(-\frac{i}{\hbar} H dt\right) \rho(t) \exp\left(\frac{i}{\hbar} H dt\right) \quad (14)$$

where  $H$  is defined in Eq. (4), and

$$\rho(t = 0) = |\Psi_{initial}\rangle \langle \Psi_{initial}| \quad (15)$$

where  $|\Psi_{initial}\rangle$  is defined in Eq. (12).

In addition to being crucial for solving differential equations, the matrix exponential is also important for control theory, transportation and waveguides. The articles [51, 52] has examined 19 different ways to compute the matrix exponential and their drawbacks, and the fact that the exponential problem has not yet been fully resolved illustrates how important it is. Zhong Wanxie proposed the precise time step integration method (PTSIM) of matrix exponential in 1991 [53]. This method avoids computer truncation errors caused by fine division and improves the numerical solution of matrix exponential to computer accuracy. This method was quickly applied to solving mathematical and physical problems [54–57]. When solving the equations of motion using stepwise integration, the matrix exponential operation involved is  $e^{A\Delta t}$ . According to the addition theorem of matrix exponential

$$e^{A\Delta t} = \left[ e^{A \frac{\Delta t}{2^M}} \right]^{2^M} = [e^{A\varepsilon}]^{2^M} \quad (16)$$

where  $A$  is matrix,  $\Delta t$  is time step,  $\varepsilon = \frac{\Delta t}{2^M}$  (usually  $M$  is taken to be equal to 20). The matrix exponential can be approximated using Taylor series expansion (4 terms)

$$e^{A\varepsilon} \approx I + A\varepsilon + \frac{(A\varepsilon)^2}{2!} + \frac{(A\varepsilon)^3}{3!} + \frac{(A\varepsilon)^4}{4!} \quad (17)$$

where  $I$  is unit matrix, then

$$\begin{aligned} e^{A\Delta t} &\approx \left[ I + A\varepsilon + \frac{(A\varepsilon)^2}{2!} + \frac{(A\varepsilon)^3}{3!} + \frac{(A\varepsilon)^4}{4!} \right]^{2^M} \\ &= [I + T_{a,0}]^{2^M} \end{aligned} \quad (18)$$

where  $T_{a,0} = A\varepsilon + \frac{(A\varepsilon)^2}{2!} + \frac{(A\varepsilon)^3}{3!} + \frac{(A\varepsilon)^4}{4!}$ , then

$$\begin{aligned} [I + T_{a,0}]^{2^M} &= [(I + T_{a,0})^2]^{2^{M-1}} \\ &= [I + 2T_{a,0} + T_{a,0}T_{a,0}]^{2^{M-1}} \\ &= [I + T_{a,1}]^{2^{M-1}} \\ &= [I + T_{a,2}]^{2^{M-2}} \\ &\dots\dots \\ &= [I + T_{a,M}] \end{aligned} \quad (19)$$

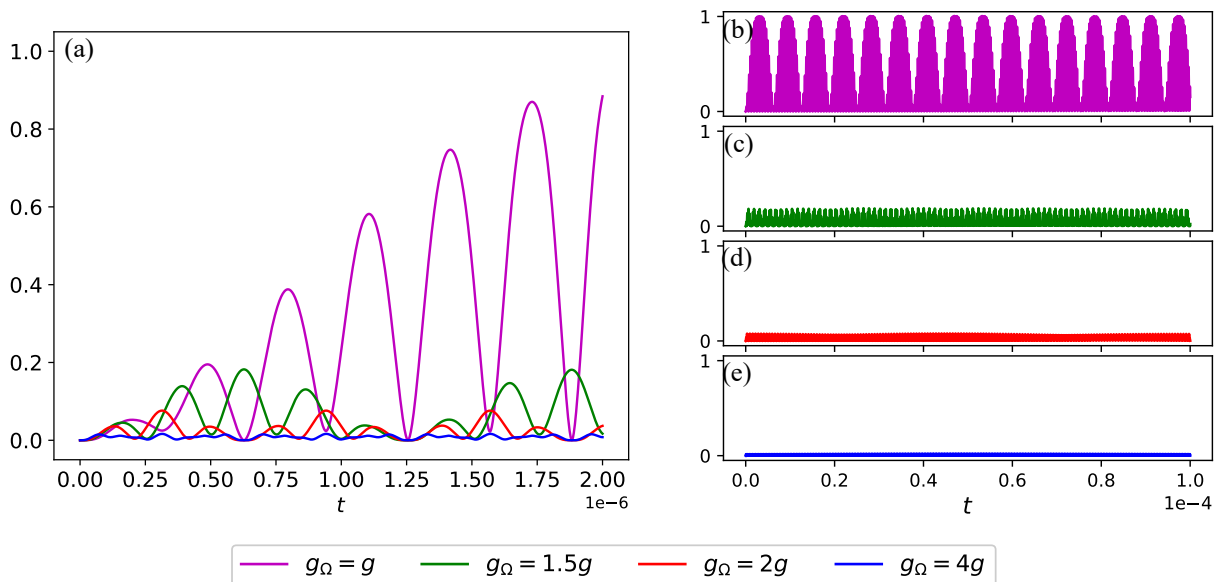


FIG. 3. (online color) *Effect of different strengths of electronic transition  $g_\Omega$  on entropy.* The magenta, green, red and blue curves, respectively, stand for different electronic transition strengths.

where  $T_{a,n} = 2T_{a,n-1} + T_{a,n-1}T_{a,n-1}$ ,  $n \geq 1$ . The above calculation process avoids operations between values with large differences in magnitude and avoids the impact of rounding errors.

## B. Quantum entropy

For a bipartite system, we set the one subsystem as  $\mathcal{A}$  and the another subsystem as  $\mathcal{B}$ . We exclusively address the entanglement in the non-dissipative situation in simulations. Quantum entropy was first introduced by von Neumann [2]. Its status is equivalent to that of Shannon entropy in classical information theory. It is the most basic and important concept in the fields of quantum information and quantum communication. From a thermodynamic point of view, the entropy of a closed system is a time-independent constant. This means that if a closed system is prepared in a pure (mixed) state, it will remain in a pure (mixed) state during the time evolution. But people are more interested in the interaction between a system and its surrounding environment, or the interaction between subsystems in a system. The density matrix describing the whole system cannot directly display the dynamics of each subsystem, so a statistical operator is needed to describe the subsystem. This is the reduced density operator of the subsystem, which can define the entropy of the subsystem and describe the dynamics of the subsystem. The von Neumann entropy of reduced density matrix, which is used to measure quantum correlation [58, 59], can be used directly when the quantum system is closed and the entire system is in the pure state  $|pure\rangle$ . However, in this case, it can also be thought

of as the entropy of entanglement. In this case, due to the Schmidt decomposition, the von Neumann entropy of each of two subsystems  $\mathcal{A}$  and  $\mathcal{B}$  can be used as a gauge of the system's entanglement [60]

$$E = S(\mathcal{A}) = S(\mathcal{B}) \quad (20)$$

where  $S(\mathcal{A})$ ,  $S(\mathcal{B})$  are corresponding to  $\rho_{\mathcal{A}}$ ,  $\rho_{\mathcal{B}}$ , respectively. And  $\rho_{\mathcal{A}(\mathcal{B})}$  — reduction of density matrix  $\rho_{AB} = |pure\rangle\langle pure|$ , which is the density matrix of whole system, has the following form

$$\begin{aligned} \rho_{\mathcal{A}} &= Tr_{\mathcal{B}}(\rho_{AB}) \\ &= \sum_b (I_{\mathcal{A}} \otimes \langle b|_{\mathcal{B}}) \rho_{AB} (I_{\mathcal{A}} \otimes |b\rangle_{\mathcal{B}}) \end{aligned} \quad (21a)$$

$$\begin{aligned} \rho_{\mathcal{B}} &= Tr_{\mathcal{A}}(\rho_{AB}) \\ &= \sum_a (\langle a|_{\mathcal{A}} \otimes I_{\mathcal{B}}) \rho_{AB} (|a\rangle_{\mathcal{A}} \otimes I_{\mathcal{B}}) \end{aligned} \quad (21b)$$

where  $Tr_{\mathcal{A},\mathcal{B}}$  represents the trace operation on the variables of the subsystem. Some details for calculating reduced density matrix and its matrix form are shown in Appx. C.

In quantum theory, the definition of von Neumann entropy of reduced density matrix  $\rho_{\mathcal{A}(\mathcal{B})}$ , called quantum reduced entropy, is as follows

$$S(\mathcal{A}(\mathcal{B})) = -Tr(\rho_{\mathcal{A}(\mathcal{B})} \log_2 \rho_{\mathcal{A}(\mathcal{B})}) \quad (22)$$

In terms of eigenvalues, we have

$$S(\mathcal{A}(\mathcal{B})) = -\sum_i \lambda_i^{\mathcal{A}(\mathcal{B})} \log_2 \lambda_i^{\mathcal{A}(\mathcal{B})} \quad (23)$$

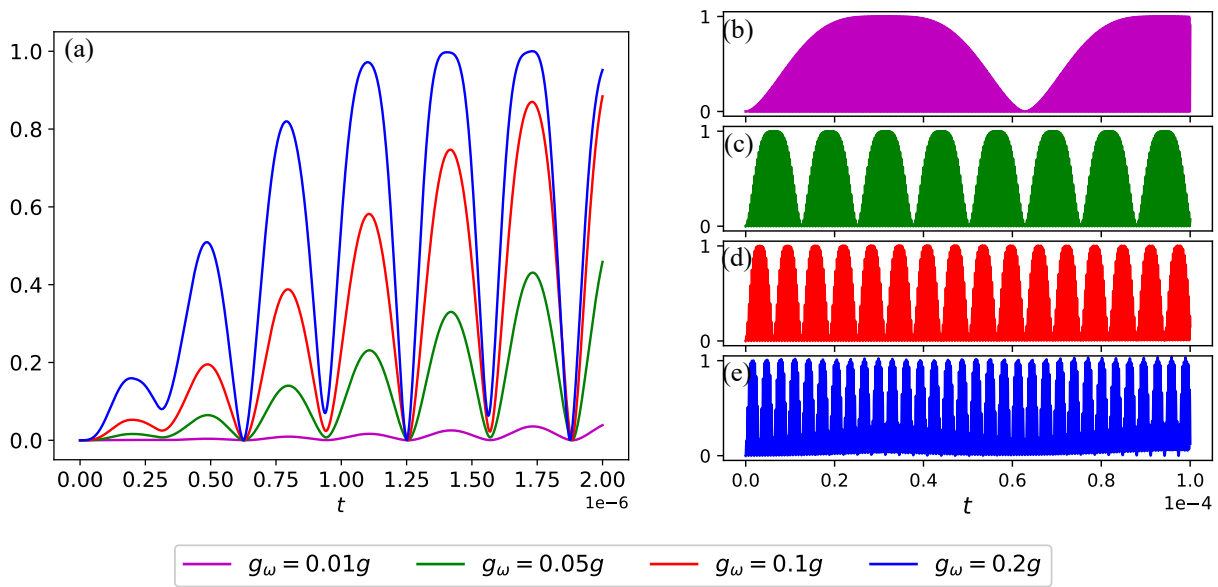


FIG. 4. (online color) *Effect of different strengths of covalent bond formation  $g_\omega$  on entropy.* The magenta, green, red and blue curves, respectively, stand for different covalent bond formation strengths.

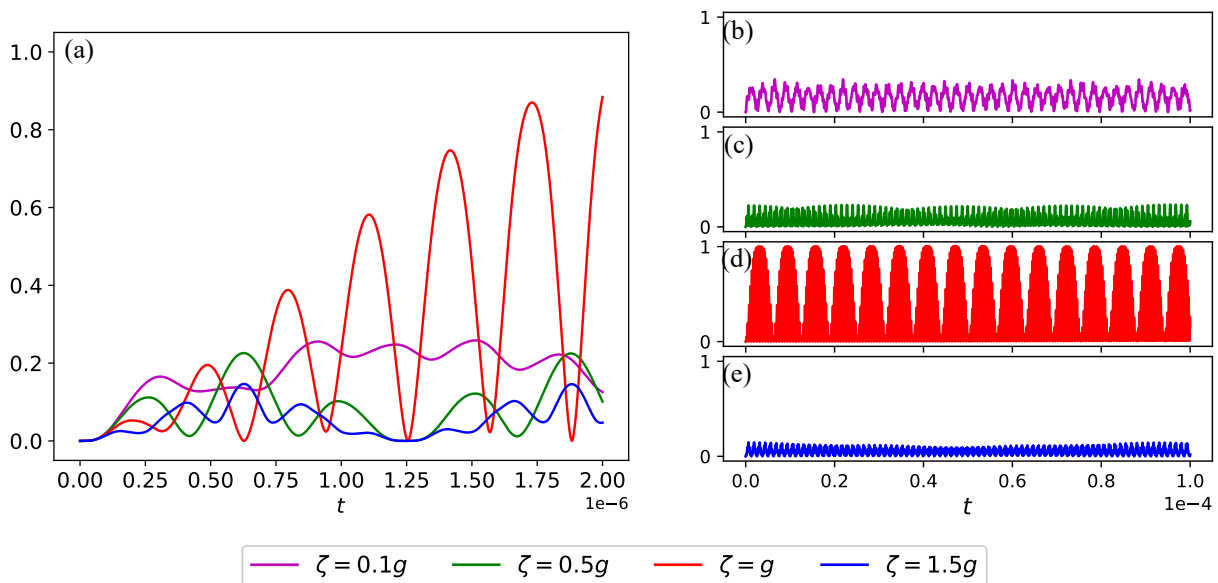


FIG. 5. (online color) *Effect of different tunneling effect strengths  $\zeta$  on entropy.* The magenta, green, red and blue curves, respectively, stand for different tunneling effect strengths.

where  $\lambda_i^{\mathcal{A}(\mathcal{B})}$  — eigenvalues of density matrix  $\rho_{\mathcal{A}(\mathcal{B})}$ .  $0 \leq S(\mathcal{A}(\mathcal{B})) \leq \log_2 N$ ,  $N = 2^n$ ,  $N$  — Hilbert space dimension,  $n$  — number of qubits of subsystem.  $S(\mathcal{A}(\mathcal{B})) = 0$  — separable state,  $S(\mathcal{A}(\mathcal{B})) > 0$  — entangled state,  $S(\mathcal{A}(\mathcal{B})) = \log_2 N$  — maximum entangled state.

#### IV. SIMULATIONS AND RESULTS

Our simulations consist of two parts: the effect of the interactions on the entropy shown in Sec. IV A and the comparison of the entropy of different subsystems shown in Sec. IV B. In this paper we consider and fix following conditions in all simulations:  $\hbar = 1$ ,  $\Omega^\uparrow = \Omega^\downarrow = 10^9$ ,  $\omega = 10^8$ ,  $g = 10^7$ .

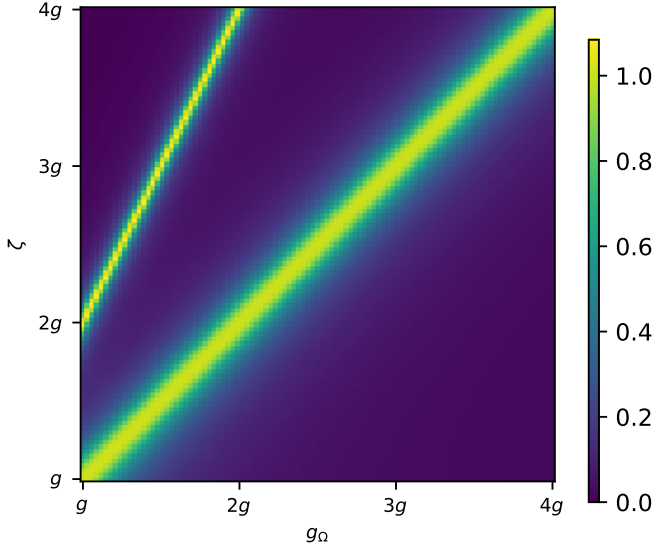


FIG. 6. (online color) *Effect of different  $g_\Omega$  and  $\zeta$  on entropy.* Each point represents the maximum of entropy of unitary evolution under the corresponding  $g_\Omega$  and  $\zeta$ .

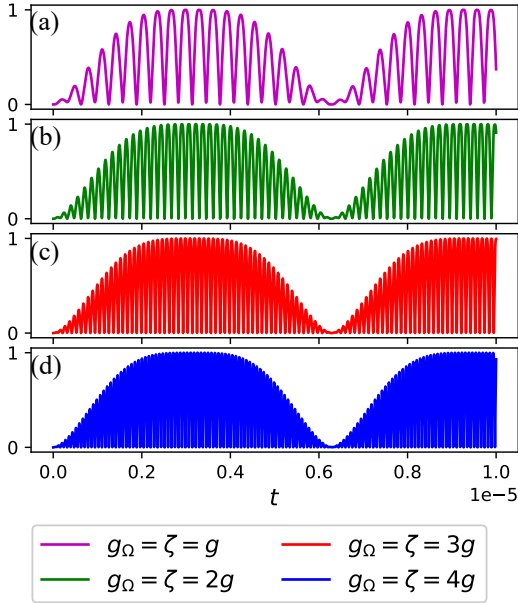


FIG. 7. (online color) *Effect of different  $g_\Omega$  and  $\zeta$  on entropy when  $\zeta = g_\Omega$ .* (a)  $\zeta = g_\Omega = g$  (magenta); (b)  $\zeta = g_\Omega = 2g$  (green); (c)  $\zeta = g_\Omega = 3g$  (red); (d)  $\zeta = g_\Omega = 4g$  (blue).

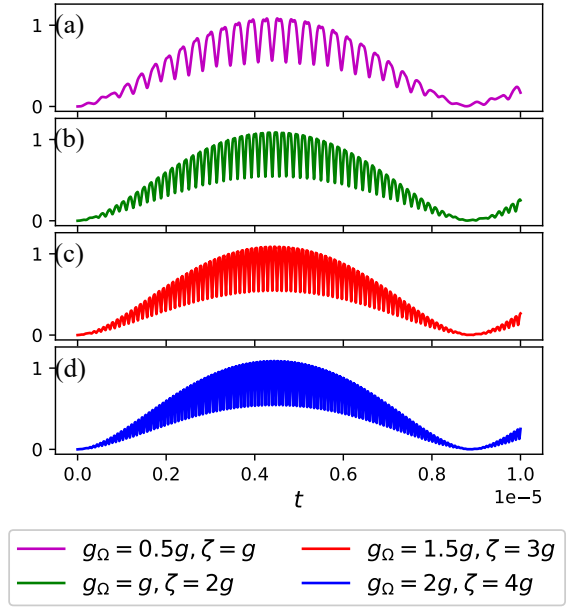


FIG. 8. (online color) *Effect of different  $g_\Omega$  and  $\zeta$  on entropy when  $\zeta = 2g_\Omega$ .* (a)  $\zeta = g$ ,  $g_\Omega = 0.5g$  (magenta), (b)  $\zeta = 2g$ ,  $g_\Omega = g$  (green), (a)  $\zeta = 3g$ ,  $g_\Omega = 1.5g$  (red), (a)  $\zeta = 4g$ ,  $g_\Omega = 2g$  (blue).

#### A. Effect of interactions on entropy

We divide the whole system into the following two subsystems

$$|\Psi\rangle_c = \underbrace{|p_1\rangle_{\Omega^\dagger}|p_2\rangle_{\Omega^\dagger}}_{\mathcal{A}} \underbrace{|m\rangle_\omega|l_1\rangle_{\Phi_1^\dagger}|l_2\rangle_{\Phi_1^\dagger}|L\rangle_{cb}|k\rangle_n}_{\mathcal{B}} \quad (24)$$

where  $\mathcal{A}$  is a subsystem composed of photons,  $\mathcal{B}$  is a system composed of matter. We define  $S_\Omega = S(\mathcal{A}) = S(\mathcal{B})$ . We will study the effect of different values of  $g_\Omega$ ,  $g_\omega$ ,  $\zeta$  on entropy  $S_\Omega$ .

Firstly, we focus on the effect of electronic transition  $g_\Omega$  on entropy. We suppose  $g_\omega = 0.1g$ ,  $\zeta = g$ . Four different values of  $g_\Omega$  are  $g$ ,  $1.5g$ ,  $2g$  and  $4g$ . The time-dependent curve of entropy takes on a wave packet-like shape. In Fig. 3 (a), we find that the greater the strength, the lower the peak value of entropy. When  $g_\Omega$  equal to  $g$ , the peak value is approximately equal to 1, and when  $g_\Omega$  is equal to  $4g$ , the peak value is close to 0. And in the four cases, the wave packets of entropy are not synchronized. In Fig. 3 (b~e), we study the envelope of wave packet. We find that the greater the strength, the lower the maximum value of the envelope of the wave packet and the shorter its period.

Secondly, we focus on the effect of covalent bond formation  $g_\omega$  on entropy. We suppose  $g_\Omega = g$ ,  $\zeta = g$ . Four different values of  $g_\omega$  are  $0.01g$ ,  $0.05g$ ,  $0.1g$  and  $0.2g$ . In Fig. 4 (a), we find that different from Fig. 3 (a), the oscillation frequencies of the entropy wave packets in these four cases are synchronized. In Fig. 4 (b~e), we find

that peak value in these four cases are almost the same and equal to 1. However, the envelopes of wave packet are different. Obviously, the length of the period of envelope is strictly inversely proportional to the size of value of  $g_\omega$ .

Thirdly, we focus on the effect of tunneling effect  $\zeta$  on entropy. We suppose  $g_\Omega = g$ ,  $g_\omega = 0.1g$ . Four different values of  $\zeta$  are  $0.1g$ ,  $0.5g$ ,  $g$  and  $1.5g$ . In Fig. 5 (a), in the four cases, the wave packets of entropy are not synchronized as same as Fig. 3 (a). Moreover, when  $\zeta = g$ , the peak value of entropy is maximum. In Fig. 5 (b~e), we can more obviously find that the peak value of entropy changes with the change of value of  $\zeta$ , and when  $\zeta = g$ , the peak value reaches a maximum of 1. In addition, the length of the period of envelope also changes with the change of value of  $\zeta$ : the period reaches its maximum value when  $\zeta = g$ .

Now we find that all electron transition strength, covalent bond formation strength and tunneling effect strength can affect the von Neumann entropy, so next we study the effect on entropy between electron transition and tunneling effect (see Fig. 6), between covalent bond formation and tunneling effect (see Fig. 9), between electron transition and covalent bond formation with two different cases (see Figs. 11 and 12). In these figures, each point represents the maximum of entropy of unitary evolution under the corresponding strengths.

Firstly, we investigate the effect on entropy of different electron transition strength and tunneling effect strength. Here  $g_\omega = 0.1g$ . In Fig. 6, there are two obvious ridges on this figure. One is when  $\zeta = g_\Omega$ , the local maximum of points obtained on this ridge is equal to 1, the another is when  $\zeta = 2g_\Omega$ , the local maximum of points obtained on this ridge is greater than 1. Interestingly, when we plot the time-evolution curves of the above two cases, we get two different wave packet types, shown in Figs. 7 and 8, respectively. Comparing these two figures, we can find that the envelope period of the wave packet in Fig. 7 is shorter than that in Fig. 8. In addition, when  $\zeta = 2g_\Omega$ , the wave packet presents a bow shape: that is, the entropy will be equal to 0 only at the initial stage and the end stage of the envelope period.

Secondly, we investigate the effect on entropy of different covalent bond formation strength and tunneling effect strength. Here  $g_\Omega = g$ . In Fig. 9, there are two emission-like beams from left to right, and the local maximum of points is concentrated in these two beams. As  $g_\omega$  becomes larger, the divergence of these two beams increases, and two beams cross at the right end of figure. Similar to Fig. 6, when  $\zeta = g$  and  $\zeta = 2g$ , two ridges are obtained respectively, and local maximum of points are obtained on these ridges. When  $\zeta = g_\Omega = g$ , the local maximum of points obtained on this ridge is equal to 1, and when  $\zeta = 2g_\Omega = 2g$ , the local maximum of points obtained on the ridge is greater than 1. For the first case, we plot the time-evolution curves in Fig. 4, and now we plot the time-evolution curves of the second case in Fig. 10. Comparing these two figures, we can find that the

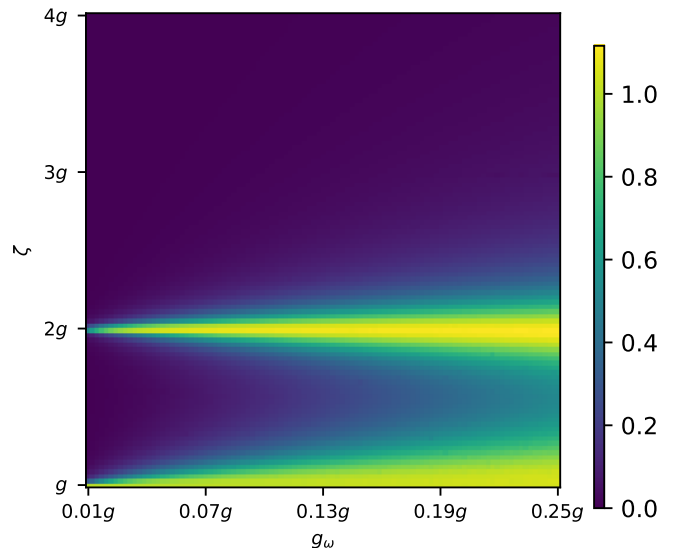


FIG. 9. (online color) *Effect of different  $g_\omega$  and  $\zeta$  on entropy.* Each point represents the maximum of entropy of unitary evolution under the corresponding  $g_\omega$  and  $\zeta$ .

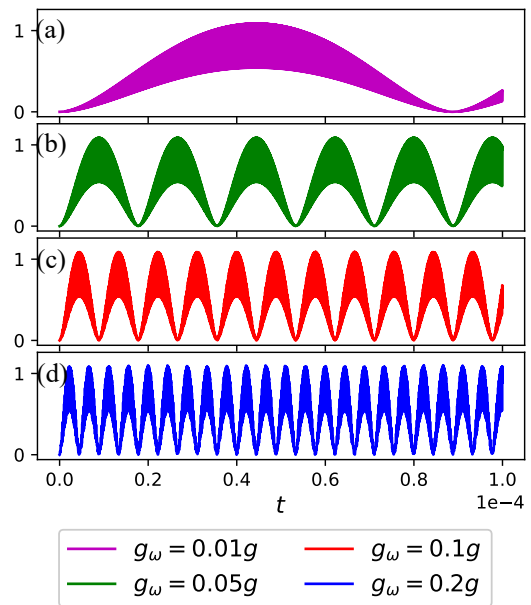


FIG. 10. (online color) *Effect of different  $g_\omega$  and  $\zeta$  on entropy when  $\zeta = 2g$ .* (a)  $g_\omega = 0.01g$  (magenta), (b)  $g_\omega = 0.05g$  (green), (c)  $g_\omega = 0.1g$  (red), (d)  $g_\omega = 0.2g$  (blue).

envelope period of the wave packet in Fig. 4 is shorter than that in Fig. 10, too. Similarly, the length of the period of envelope in Fig. 10 is strictly inversely proportional to the size of value of  $g_\omega$ , and when  $\zeta = 2g_\Omega = 2g$ , the wave packet also presents a bow shape.

Thirdly, we investigate the effect on entropy of different

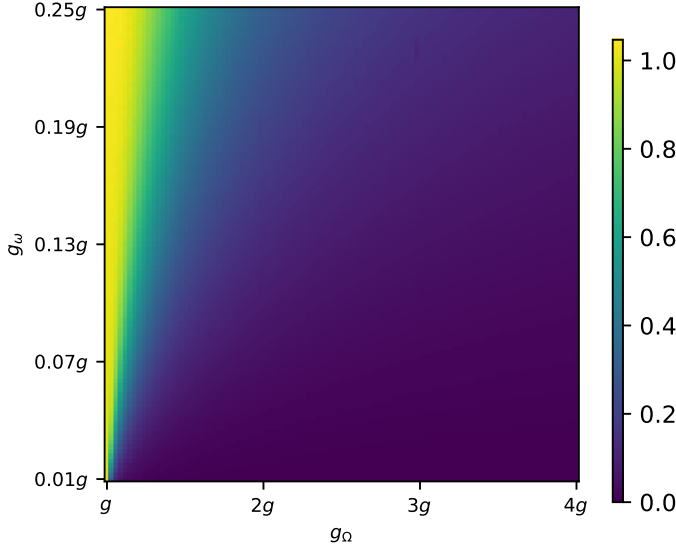


FIG. 11. (online color) *Effect of different  $g_\Omega$  and  $g_\omega$  on entropy when  $\zeta = g$ .* Each point represents the maximum of entropy of unitary evolution under the corresponding  $g_\Omega$  and  $g_\omega$ .

electron transition strength and covalent bond formation strength. Considering that  $\zeta = g$  and  $\zeta = 2g$  have different effects on entropic dynamics above, we study the effects of different  $g_\Omega$  and  $g_\omega$  on entropy at the same time in these two cases. Thus, when  $\zeta = g$ , Fig. 11 is obtained. We can find that there is an emission-like beam from bottom to top at the left end. When  $\zeta = g_\Omega = g$ , local maximum of points are obtained. In Fig. 12, when  $\zeta = 2g$ , we can find that there are two emission-like beams from bottom to top at both the left and right ends. When  $\zeta = 2g_\Omega = 2g$ , local maximum of points are obtained at the left end, and when  $\zeta = g_\Omega = 2g$ , local maximum of points are obtained at the right of the first emission-like beam. Different from the two clear ridges in Fig. 6, the reason for the emission-like beam shape in Figs. 11 and 12 is the increase in  $g_\omega$ .

### B. Comparison of entropy of different subsystems

We assume the following situations in Fig. 13

$$|\Psi\rangle_C = \underbrace{|p_1\rangle_{\Omega^\uparrow}}_A \underbrace{|p_2\rangle_{\Omega^\downarrow} |m\rangle_\omega |l_1\rangle_{\Phi_1^\uparrow} |l_2\rangle_{\Phi_1^\downarrow} |L\rangle_{cb} |k\rangle_n}_B \quad (25)$$

where  $\mathcal{A}$  is a subsystem composed of photon with mode  $\Omega^\uparrow$ , and

$$|\Psi\rangle_C = \underbrace{|p_1\rangle_{\Omega^\uparrow} |p_2\rangle_{\Omega^\downarrow} |m\rangle_\omega}_B \underbrace{|l_1\rangle_{\Phi_1^\uparrow} |l_2\rangle_{\Phi_1^\downarrow} |L\rangle_{cb} |k\rangle_n}_B \quad (26)$$

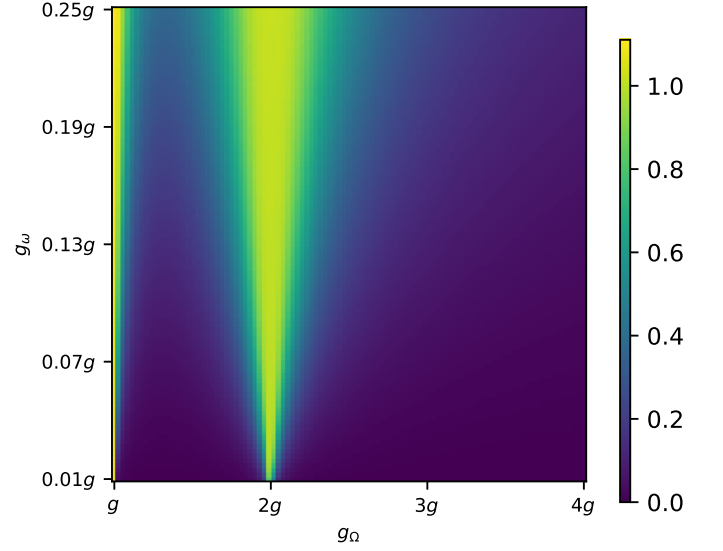


FIG. 12. (online color) *Effect of different  $g_\Omega$  and  $g_\omega$  on entropy when  $\zeta = 2g$ .* Each point represents the maximum of entropy of unitary evolution under the corresponding  $g_\Omega$  and  $g_\omega$ .

where  $\mathcal{A}$  is a subsystem composed of photon with mode  $\Omega^\downarrow$ . We define  $S_{\Omega^\uparrow}$ ,  $S_{\Omega^\downarrow}$  are entropies corresponding to photon with mode  $\Omega^\uparrow$  and photon with mode  $\Omega^\downarrow$ , respectively.

In Fig. 13, we get the following relational expression

$$S_{\Omega^\uparrow} + S_{\Omega^\downarrow} \geq S_\Omega \geq S_{\Omega^\uparrow} = S_{\Omega^\downarrow} \quad (27)$$

where  $S_{\Omega^\uparrow}$  always coincides with  $S_{\Omega^\downarrow}$  since our quantum system is symmetrical, and the result satisfies that the sum of the entropies of the two subsystems  $S_{\Omega^\uparrow} + S_{\Omega^\downarrow}$  is greater than the entire entropy of these subsystems  $S_\Omega$ . In Fig. 13 (b), we can find that the wave packet envelopes of  $S_\Omega$ ,  $S_{\Omega^\uparrow}$ ,  $S_{\Omega^\downarrow}$  are all synchronized.

We assume the following situations in Fig. 14

$$|\Psi\rangle_C = \underbrace{|p_1\rangle_{\Omega^\uparrow} |p_2\rangle_{\Omega^\downarrow}}_B \underbrace{|m\rangle_\omega}_A \underbrace{|l_1\rangle_{\Phi_1^\uparrow} |l_2\rangle_{\Phi_1^\downarrow} |L\rangle_{cb} |k\rangle_n}_B \quad (28)$$

where  $\mathcal{A}$  is a subsystem composed of phonon with mode  $\omega$ , and

$$|\Psi\rangle_C = \underbrace{|p_1\rangle_{\Omega^\uparrow} |p_2\rangle_{\Omega^\downarrow} |m\rangle_\omega}_A \underbrace{|l_1\rangle_{\Phi_1^\uparrow} |l_2\rangle_{\Phi_1^\downarrow} |L\rangle_{cb} |k\rangle_n}_B \quad (29)$$

where  $\mathcal{A}$  is a subsystem composed of photons and phonon. We define  $S_\omega$  is entropy corresponding to phonon with mode  $\omega$ ,  $S_{\Omega+\omega}$  is entropy corresponding to photons and phonon.

In Fig. 14, we get the following relational expression

$$S_\Omega + S_\omega \geq S_{\Omega+\omega} \geq S_\omega \geq S_\Omega \quad (30)$$

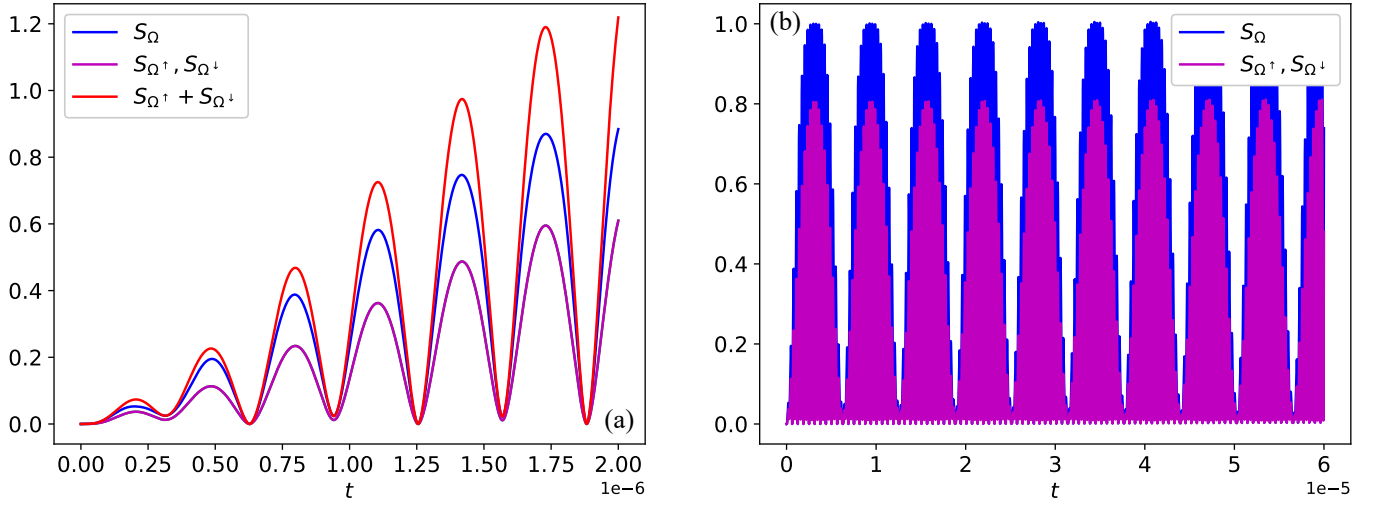


FIG. 13. (online color) *Comparison of von Neumann entropy of different photonic states.*  $S_{\Omega^\dagger}$  is entropy of photon with mode  $\Omega^\dagger$ ,  $S_{\Omega^\ddagger}$  is entropy of photon with mode  $\Omega^\ddagger$ ,  $S_\Omega$  is entropy of both two types of photon.

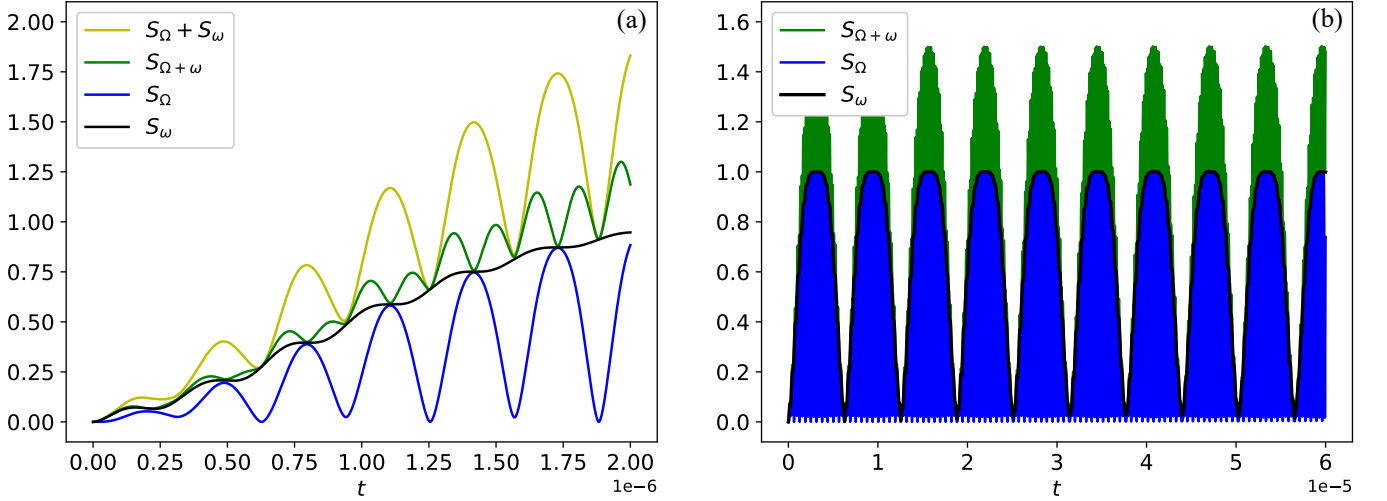


FIG. 14. (online color) *Comparison of von Neumann entropy between photonic state and phononic state.*  $S_\omega$  is entropy of phonon with mode  $\omega$ .

where the sum of the entropies of the two subsystems  $S_\Omega + S_\omega$  is greater than the entire entropy of these subsystems  $S_{\Omega+\omega}$ . In particular, the wave packets of  $S_\omega$ ,  $S_{\Omega+\omega}$  and  $S_\Omega + S_\omega$  are bow-shaped. This means that all time-dependent curves of the entropy of subsystems containing phonons have bow shape. In Fig. 14 (b), we can find that the envelopes of  $S_{\Omega+\omega}$ ,  $S_\Omega$ ,  $S_\omega$  are all synchronized.

## V. CONCLUDING DISCUSSION AND FUTURE WORK

In this paper, we explore various aspects of entropy of a multiqubit cavity QED system. The entropic dynamics has been constructed, and several analytical findings have been drawn from it:

In Sec. IV A, according to results from Figs. 3, 4 and 5, we proved that  $g_\Omega$  and  $\zeta$  affect significantly the peak value of entropy, but  $g_\omega$  affects slightly that. Different values of  $g_\omega$  will not affect the synchronization of wave packets, but changes in the values of  $g_\Omega$  or  $\zeta$  will affect the synchronization. According to results from Figs. 6, 9, 11 and 12, we will find that when  $\zeta$  is equal to or

twice as large as  $g_\Omega$ , the local maximum of points can be obtained. In particular, when  $\zeta$  is twice as large as  $g_\Omega$ , the entropy curves take on a bow shape (see Figs. 8 and 10). In addition, the strength of the interaction will also change the period of the wave packet envelope, unless  $g_\Omega$  and  $\zeta$  are increased in equal proportions.

In Sec. IV B, we compared the entropic dynamics between different subsystems. We obtained two inequalities between the entropies of different subsystems (see Eqs. (27), (30)), and also verified that the sum of the entropies of the two subsystems is greater than or equal to the entropy of the entire system composed of these two subsystems. We find that the wave packet of the entropy of any subsystem containing phonon exhibits a bow shape.

We tried to study the characteristics of entropy on a seven-qubit complicated quantum system and obtained

some regular results. The results show that the entropic dynamics can be controlled by selectively choosing system parameters, and some rules are obtained. These results lay the foundation for our future studies of more complicated quantum model entropy dynamics.

## ACKNOWLEDGMENTS

This work was supported by the China Scholarship Council (CSC No.202108090483). The author acknowledges Center for Collective Usage of Ultra HPC Resources (<https://www.parallel.ru/>) at Lomonosov Moscow State University for providing supercomputer resources that have contributed to the research results reported within this paper.

## Appendix A: Rotating wave approximation

RWA is taken into account in this paper. This approach ignores the quickly oscillating terms  $\sigma^\dagger a^\dagger$ ,  $\sigma a$  in a Hamiltonian. When the strength of the applied electromagnetic radiation is close to resonance with an atomic transition and the strength is low, this approximation holds true [61]. Thus,

$$\frac{g}{\hbar\omega_{cavity}} \approx \frac{g}{\hbar\omega_{atom}} \ll 1 \quad (\text{A1})$$

where  $\omega_{cavity}$  stands for cavity frequency, which includes  $\Omega_c$  ( $\Omega_c^\uparrow$  and  $\Omega_c^\downarrow$ ) for photon and  $\omega_c$  for phonon; and  $\omega_{atom}$  for transition frequency (of atom), which includes  $\Omega_a$  ( $\Omega_a^\uparrow$  and  $\Omega_a^\downarrow$ ) for electronic transition and  $\omega_a$  formation-break of covalent bond. RWA allows us to change  $(\sigma^\dagger + \sigma)(a^\dagger + a)$  to  $\sigma^\dagger a + \sigma a^\dagger$ . In Eq. (4) we typically presume that  $\Omega_{cavity} = \Omega_{atom}$ :  $\Omega_c = \Omega_a = \Omega$  ( $\Omega_c^\uparrow = \Omega_a^\uparrow = \Omega^\uparrow$  and  $\Omega_c^\downarrow = \Omega_a^\downarrow = \Omega^\downarrow$ ),  $\omega_c = \omega_a = \omega$ .

## Appendix B: Matrix form of operators

The matrix form of annihilation and creation operators  $a$  and  $a^\dagger$  in Eq. (4) are described as follows

$$a = \begin{matrix} |0\rangle \\ |1\rangle \\ |2\rangle \\ \vdots \\ \vdots \\ |p-2\rangle \\ |p-1\rangle \\ |p\rangle \end{matrix} \begin{pmatrix} 0 & 1 & 0 & \cdots & \cdots & 0 & 0 & 0 \\ 0 & 0 & \sqrt{2} & \cdots & \cdots & 0 & 0 & 0 \\ 0 & 0 & 0 & \cdots & \cdots & 0 & 0 & 0 \\ \vdots & \vdots & \vdots & \ddots & \ddots & \vdots & \vdots & \vdots \\ \vdots & \vdots & \vdots & \ddots & \ddots & \vdots & \vdots & \vdots \\ 0 & 0 & 0 & \cdots & \cdots & 0 & \sqrt{p-1} & 0 \\ 0 & 0 & 0 & \cdots & \cdots & 0 & 0 & \sqrt{p} \\ 0 & 0 & 0 & \cdots & \cdots & 0 & 0 & 0 \end{pmatrix} \quad (\text{B1a})$$

$$a^\dagger = \begin{matrix} |0\rangle \\ |1\rangle \\ |2\rangle \\ \vdots \\ \vdots \\ |p-2\rangle \\ |p-1\rangle \\ |p\rangle \end{matrix} \begin{pmatrix} 0 & 0 & 0 & \cdots & \cdots & 0 & 0 & 0 \\ 1 & 0 & 0 & \cdots & \cdots & 0 & 0 & 0 \\ 0 & \sqrt{2} & 0 & \cdots & \cdots & 0 & 0 & 0 \\ \vdots & \vdots & \vdots & \ddots & \ddots & \vdots & \vdots & \vdots \\ \vdots & \vdots & \vdots & \ddots & \ddots & \vdots & \vdots & \vdots \\ 0 & 0 & 0 & \cdots & \cdots & 0 & 0 & 0 \\ 0 & 0 & 0 & \cdots & \cdots & \sqrt{p-1} & 0 & 0 \\ 0 & 0 & 0 & \cdots & \cdots & 0 & \sqrt{p} & 0 \end{pmatrix} \quad (\text{B1b})$$

where  $p$  can be replaced by  $p_1$ ,  $p_2$  and  $m$  in this paper. And the matrix form of relaxation and excitation operators  $\sigma$  and  $\sigma^\dagger$  in Eq. (4) are described as follows

$$\sigma = \begin{matrix} |0\rangle \\ |1\rangle \end{matrix} \begin{pmatrix} 0 & 1 \\ 0 & 0 \end{pmatrix} \quad (\text{B2a})$$

$$\sigma^\dagger = \begin{matrix} |0\rangle \\ |1\rangle \end{matrix} \begin{pmatrix} 0 & 0 \\ 1 & 0 \end{pmatrix} \quad (\text{B2b})$$

In this paper, operators  $\sigma_{\Omega^\uparrow}$ ,  $\sigma_{\Omega^\downarrow}$ ,  $\sigma_\omega$  and  $\sigma_n$ , and their conjugate operators all obey the rule of Eq. (B2).

### Appendix C: Reduced density matrix

For reduced density matrix, we usually have three types of it: left-end reduced, right-end reduced and intermediate reduced, which are corresponding to these three following cases

$$|\Psi\rangle_C = \underbrace{|\cdots\rangle}_A |\cdots\rangle \quad (\text{C1a})$$

$$|\Psi\rangle_C = |\cdots\rangle \underbrace{|\cdots\rangle}_A \quad (\text{C1b})$$

$$|\Psi\rangle_C = |\cdots\rangle \underbrace{|\cdots\rangle}_A |\cdots\rangle \quad (\text{C1c})$$

Let's give an example of three-qubit system, having following Hilbert space

$$|\Psi\rangle_C = |x\rangle_0 |y\rangle_1 |z\rangle_2 \quad (\text{C2})$$

where  $x, y, z \in \{0, 1\}$ . And the density matrix is as follows

$$\rho_{012} = \begin{matrix} |000\rangle \\ |001\rangle \\ |010\rangle \\ |011\rangle \\ |100\rangle \\ |101\rangle \\ |110\rangle \\ |111\rangle \end{matrix} \begin{pmatrix} a_{00} & a_{01} & a_{02} & a_{03} & a_{04} & a_{05} & a_{06} & a_{07} \\ a_{10} & a_{11} & a_{12} & a_{13} & a_{14} & a_{15} & a_{16} & a_{17} \\ a_{20} & a_{21} & a_{22} & a_{23} & a_{24} & a_{25} & a_{26} & a_{27} \\ a_{30} & a_{31} & a_{32} & a_{33} & a_{34} & a_{35} & a_{36} & a_{37} \\ a_{40} & a_{41} & a_{42} & a_{43} & a_{44} & a_{45} & a_{46} & a_{47} \\ a_{50} & a_{51} & a_{52} & a_{53} & a_{54} & a_{55} & a_{56} & a_{57} \\ a_{60} & a_{61} & a_{62} & a_{63} & a_{64} & a_{65} & a_{66} & a_{67} \\ a_{70} & a_{71} & a_{72} & a_{73} & a_{74} & a_{75} & a_{76} & a_{77} \end{pmatrix} \quad (\text{C3})$$

We will separately find the reduced density matrices  $\rho_0$ ,  $\rho_1$  and  $\rho_2$ . Firstly, according to Eq. (21a), reduced density matrix  $\rho_{01}$  has following matrix form

$$\rho_{01} = \begin{matrix} |00\rangle \\ |01\rangle \\ |10\rangle \\ |11\rangle \end{matrix} \begin{pmatrix} a_{00} + a_{11} & a_{02} + a_{13} & a_{04} + a_{15} & a_{06} + a_{17} \\ a_{20} + a_{31} & a_{22} + a_{33} & a_{24} + a_{35} & a_{26} + a_{37} \\ a_{40} + a_{51} & a_{42} + a_{53} & a_{44} + a_{55} & a_{46} + a_{57} \\ a_{60} + a_{71} & a_{62} + a_{73} & a_{64} + a_{75} & a_{66} + a_{77} \end{pmatrix} \quad (\text{C4})$$

Immediately followed,  $\rho_0$  has following matrix form

$$\rho_0 = \begin{matrix} |0\rangle \\ |1\rangle \end{matrix} \begin{pmatrix} a_{00} + a_{11} + a_{22} + a_{33} & a_{04} + a_{15} + a_{26} + a_{37} \\ a_{40} + a_{51} + a_{62} + a_{73} & a_{44} + a_{55} + a_{66} + a_{77} \end{pmatrix} \quad (\text{C5})$$

Then, according to Eq. (21b), reduced density matrix  $\rho_{12}$  has following matrix form

$$\rho_{12} = \begin{matrix} |00\rangle \\ |01\rangle \\ |10\rangle \\ |11\rangle \end{matrix} \begin{pmatrix} a_{00} + a_{44} & a_{01} + a_{45} & a_{02} + a_{46} & a_{03} + a_{47} \\ a_{10} + a_{54} & a_{11} + a_{55} & a_{12} + a_{56} & a_{13} + a_{57} \\ a_{20} + a_{64} & a_{21} + a_{65} & a_{22} + a_{66} & a_{23} + a_{67} \\ a_{30} + a_{74} & a_{31} + a_{75} & a_{32} + a_{76} & a_{33} + a_{77} \end{pmatrix} \quad (\text{C6})$$

Immediately followed,  $\rho_2$  has following matrix form

$$\rho_2 = \begin{array}{l} |0\rangle \\ |1\rangle \end{array} \begin{pmatrix} a_{00} + a_{44} + a_{22} + a_{66} & a_{01} + a_{45} + a_{23} + a_{67} \\ a_{10} + a_{54} + a_{32} + a_{76} & a_{11} + a_{55} + a_{33} + a_{77} \end{pmatrix} \quad (\text{C7})$$

In Eq. (C6),  $\rho_{12}$  is obtained by applying Eq. (21b). Next, by applying Eq. (21a), reduced density matrix  $\rho_1$  is reduced from  $\rho_{12}$

$$\rho_1 = \begin{array}{l} |0\rangle \\ |1\rangle \end{array} \begin{pmatrix} a_{00} + a_{44} + a_{11} + a_{55} & a_{02} + a_{46} + a_{13} + a_{57} \\ a_{20} + a_{64} + a_{31} + a_{75} & a_{22} + a_{66} + a_{33} + a_{77} \end{pmatrix} \quad (\text{C8})$$

For obtaining  $\rho_1$ , we can use another method: swapping the qubits' positions. For example, the Eq. (C2) can be rewritten as

$$|\Psi\rangle_{\mathcal{C}'} = |y\rangle_1 |x\rangle_0 |z\rangle_2 \quad (\text{C9})$$

where  $\mathcal{C} \neq \mathcal{C}'$ , and the new density matrix is  $\rho_{102}$ . Thus, we just apply twice the Eq. (21a), and  $\rho_1$  is obtained. Here  $\rho_{01}$  and  $\rho_0$  are left-end reduced density matrices,  $\rho_{12}$  and  $\rho_2$  — right-end reduced,  $\rho_1$  — intermediate reduced.

Process of obtaining these three types of reduced density matrix has obvious regularities. We can extend them to the seven-qubit system, then each reduced density matrix  $\mathcal{A}$  from Eqs. (24), (25), (26), (28) and (29) can be obtained.

#### Appendix D: Abbreviations and notations

See Tab. II.

TABLE II: List of abbreviations and notations used in this paper.

Abbreviations/Notations	Descriptions
QED	Quantum electrodynamics
JCM	Jaynes–Cummings model
TCM	Tavis–Cummings model
JCHM	Jaynes–Cummings–Hubbard model
TCHM	Tavis–Cummings–Hubbard model
QME	Quantum master equation
RWA	Rotating wave approximation
PTSIM	Precise time step integration method
$\uparrow$	Spin up
$\downarrow$	Spin down
$e$	Electron
$0_1$	Atomic excited orbital of the first atom
$0_2$	Atomic excited orbital of the second atom
$\Phi_0$	Bonding orbital or molecular ground orbital
$\Phi_1$	Antibonding orbital or molecular excited orbital
$ \Psi\rangle$	Quantum state
$\mathcal{C}$	Hilbert space
$\mathcal{C}'$	Hilbert space
$\Omega$	Transition frequency for electron in molecule (e.g. $\Omega^\uparrow$ , $\Omega^\downarrow$ )
$\Omega^\uparrow$	Transition frequency for electron with $\uparrow$ in molecule
$\Omega^\downarrow$	Transition frequency for electron with $\downarrow$ in molecule
$\omega$	Phononic mode
$cb$	Covalent bond
$n$	Nucleus
$H$	Hamiltonian
$\hbar$	Reduced Planck constant or Dirac constant
$a$	Photon (phonon) annihilation operator (e.g. $a_{\Omega^\uparrow}$ , $a_{\Omega^\downarrow}$ , $a_\omega$ ) and its hermitian conjugate operator — $a^\dagger$
$\sigma$	Interaction operator of atom with the electromagnetic field of the cavity (e.g. $\sigma_{\Omega^\uparrow}$ , $\sigma_{\Omega^\downarrow}$ , $\sigma_\omega$ , $\sigma_n$ ) and its hermitian conjugate operator — $\sigma^\dagger$
$g$	Coupling strength (e.g. $g_{\Omega^\uparrow}$ , $g_{\Omega^\downarrow}$ , $g_\omega$ )
$\zeta$	Nucleus tunnelling strength or atom leap strength

Continued on next page

– continued from previous page

Abbreviations/Notations	Descriptions
$ \Psi_{initial}\rangle$	Initial state
$\rho$	Density Matrix
$A$	Matrix
$\Delta t$	Time step
$\varepsilon$	$\varepsilon = \frac{\Delta t}{2M}$
$I$	Identity matrix
$\mathcal{A}$	Subsystems
$\mathcal{B}$	Subsystems
$S$	Entropy (e.g. $S_{\Omega}$ , $S_{\Omega^{\uparrow}}$ , $S_{\Omega^{\downarrow}}$ , $S_{\omega}$ , $S_{\Omega+\omega}$ )
$S_{\Omega}$	Entropy of subsystem composed of photons
$S_{\Omega^{\uparrow}}$	Entropy of subsystem composed of photon with mode $\Omega^{\uparrow}$
$S_{\Omega^{\downarrow}}$	Entropy of subsystem composed of photon with mode $\Omega^{\downarrow}$
$S_{\omega}$	Entropy of subsystem composed of phonon
$S_{\Omega+\omega}$	Entropy of subsystem composed of photons and phonon
$Tr$	Trace
$\rho_{\mathcal{A}}$	Reduced density matrix
$\rho_{\mathcal{B}}$	Reduced density matrix
$\lambda_i$	Eigenvalue
$N$	Hamiltonian dimension
$n$	Number of qubits
$\omega_{cavity}$	Cavity frequency
$\omega_{atom}$	Electron transition frequency

- 
- [1] S. Brush, Book 2, statistical physics and irreversible processes, in *The kind of motion we call heat : a history of the kinetic theory of gases in the 19th century* (Elsevier, Amsterdam, 1976) pp. 576–577.
- [2] J. Von Neumann, *Mathematische Grundlagen der Quantenmechanik* (Springer, 1932).
- [3] S. Phoenix and P. Knight, Fluctuations and entropy in models of quantum optical resonance, *Annals of Physics* **186**, 381 (1988).
- [4] S. J. D. Phoenix and P. L. Knight, Periodicity, phase, and entropy in models of two-photon resonance, *J. Opt. Soc. Am. B* **7**, 116 (1990).
- [5] S. J. D. Phoenix and P. L. Knight, Establishment of an entangled atom-field state in the Jaynes–Cummings model, *Phys. Rev. A* **44**, 6023 (1991).
- [6] V. Bužek, H. Moya-Cessa, P. L. Knight, and S. J. D. Phoenix, Schrödinger-cat states in the resonant Jaynes–Cummings model: Collapse and revival of oscillations of the photon-number distribution, *Phys. Rev. A* **45**, 8190 (1992).
- [7] V. Bužek and B. Hladký, Macroscopic superposition states of light via two-photon resonant interaction of atoms with cavity field, *Journal of Modern Optics* **40**, 1309 (1993).
- [8] P. L. Knight and B. W. Shore, Schrödinger-cat states of the electromagnetic field and multilevel atoms, *Phys. Rev. A* **48**, 642 (1993).
- [9] C. E. Shannon, A mathematical theory of communication, *Bell System Technical Journal* **27**, 379 (1948).
- [10] A. Einstein, B. Podolsky, and N. Rosen, Can quantum-mechanical description of physical reality be considered complete?, *Phys. Rev.* **47**, 777 (1935).
- [11] E. Schrödinger, Die gegenwärtige situation in der quantenmechanik, *Naturwissenschaften* **23**, 807 (1935).
- [12] D. A. M. Abo-Kahla and M. Abdel-Aty, Information entropy of multi-qubit Rabi system, *International Journal of Quantum Information* **13**, 1550042 (2015).
- [13] D. A. M. Abo-Kahla, Information entropies of multi-qubit Rabi model beyond the rotating wave approximation, *Nonlinear Dyn* **94**, 1689 (2018).
- [14] D. A. M. Abo-Kahla and A. Farouk, Entanglement and entropy of a three-qubit system interacting with a quantum spin environment, *Applied Sciences* **9**, 10.3390/app9235222 (2019).
- [15] C. H. Bennett, Quantum information and computation, *Physics Today* **48**, 24 (1995).
- [16] N. J. Cerf and C. Adami, Negative entropy and information in quantum mechanics, *Phys. Rev. Lett.* **79**, 5194 (1997).
- [17] V. Vedral and M. B. Plenio, Entanglement measures and purification procedures, *Phys. Rev. A* **57**, 1619 (1998).
- [18] P. Z. Mao-Fa Fang and S. Swain, Entropy squeezing for a two-level atom, *Journal of Modern Optics* **47**, 1043 (2000).
- [19] F. Mao-Fa, Z. Peng, and S. Swain, Information entropy and squeezing of quantum fluctuations in a two-level atom, *Chinese Physics Letters* **17**, 798 (2000).
- [20] W. Yao and J. Wang, Differential symbolic entropy in nonlinear dynamics complexity analysis (2018), arXiv:1801.08416 [physics.data-an].
- [21] M. Costa, A. L. Goldberger, and C.-K. Peng, Multiscale entropy analysis of complex physiologic time series, *Phys. Rev. Lett.* **89**, 068102 (2002).
- [22] C. Bandt and B. Pompe, Permutation entropy: A natural complexity measure for time series, *Phys. Rev. Lett.* **88**, 174102 (2002).
- [23] K. Keller and M. Sinn, A standardized approach to the Kolmogorov–Sinai entropy, *Nonlinearity* **22**, 2417 (2009).

- [24] A.-S. Obada, S. Abdel-Khalek, M. Ahmed, and D. Abo-Kahla, Applications of the master equation of a two-level atom in a narrow-bandwidth squeezed vacuum, *Physica A: Statistical Mechanics and its Applications* **388**, 3961 (2009).
- [25] D. Abo-Kahla and M. Abdel-Aty, Dynamics of a tri-beam laser interacting with a three-level atom, *Laser Phys* **22**, 1803 (2012).
- [26] M. Abdel-Aty, D. Abo-Kahla, and A.-S. Obada, Spatial dependence of moving three-level atoms interacting with a three-laser beam, *Canadian Journal of Physics* **91**, 1068 (2013).
- [27] C. Bandt, Permutation entropy and order patterns in long time series, in *Time Series Analysis and Forecasting*, edited by I. Rojas and H. Pomares (Springer International Publishing, Cham, 2016) pp. 61–73.
- [28] D. Abo-Kahla and M. Ahmed, Some studies of the interaction between N-two level atoms and three level atom, *Journal of the Egyptian Mathematical Society* **24**, 487 (2016).
- [29] D. Abo-Kahla, M. Ahmed, and A. Makram-Allah, Analytical solution of a three-level atom coupled to four systems of N-two-level atoms, *Opt Rev* **26**, 699 (2019).
- [30] E. A. Sete and H. Eleuch, High-efficiency quantum state transfer and quantum memory using a mechanical oscillator, *Phys. Rev. A* **91**, 032309 (2015).
- [31] N. Bogolyubov and A. Soldatov, Time-convolutionless master equation for multi-level open quantum systems with initial system-environment correlations, *Appl Math Inf Sci* **14**, 771 (2020).
- [32] M. Zidan, S. Aldulaimi, and H. Eleuch, Analysis of the quantum algorithm based on entanglement measure for classifying boolean multivariate function into novel hidden classes: Revisited, *Appl Math Inf Sci* **15**, 643 (2021).
- [33] M. Zidan, A.-H. Abdel-Aty, A. Khalil, M. Abdel-Aty, and H. Eleuch, A novel efficient quantum random access memory, *IEEE Access* **9**, 151775 (2021).
- [34] D. A. M. Abo-Kahla, M. Y. Abd-Rabbou, and N. Metwally, The orthogonality speed of two-qubit state interacts locally with spin chain in the presence of Dzyaloshinsky–Moriya interaction, *Laser Physics Letters* **18**, 045203 (2021).
- [35] H. hui Miao and W. shun Li, Entanglement and quantum discord in the cavity QED models (2024), arXiv:2307.07352 [quant-ph].
- [36] E. T. Jaynes and F. W. Cummings, Comparison of quantum and semiclassical radiation theories with application to the beam maser, *Proceedings of the IEEE* **51**, 89 (1963).
- [37] M. Tavis and F. W. Cummings, Exact solution for an N-molecule—radiation-field Hamiltonian, *Phys. Rev.* **170**, 379 (1968).
- [38] D. G. Angelakis, M. F. Santos, and S. Bose, Photon-blockade-induced mott transitions and XY spin models in coupled cavity arrays, *Phys. Rev. A* **76**, 031805 (2007).
- [39] H. Wei, J. Zhang, S. Greschner, T. C. Scott, and W. Zhang, Quantum Monte Carlo study of superradiant supersolid of light in the extended Jaynes–Cummings–Hubbard model, *Phys. Rev. B* **103**, 184501 (2021).
- [40] S. Prasad and A. Martin, Effective three-body interactions in Jaynes–Cummings–Hubbard systems, *Sci Rep* **8**, 16253 (2018).
- [41] L. Guo, S. Greschner, S. Zhu, and W. Zhang, Supersolid and pair correlations of the extended Jaynes–Cummings–Hubbard model on triangular lattices, *Phys. Rev. A* **100**, 033614 (2019).
- [42] K. C. Smith, A. Bhattacharya, and D. J. Masiello, Exact  $k$ -body representation of the Jaynes–Cummings interaction in the dressed basis: Insight into many-body phenomena with light, *Phys. Rev. A* **104**, 013707 (2021).
- [43] Y. I. Ozhigov, Space of dark states in Tavis–Cummings model, *Modern Information Technologies and IT Education* **15**, 27 (2019).
- [44] R. Düll, A. Kulagin, W. Lee, Y. Ozhigov, H. Miao, and K. Zheng, Quality of control in the Tavis–Cummings–Hubbard model, *Computational Mathematics and Modeling* **32**, 75 (2021).
- [45] A. Vitaliy, K. Zheng, K. Alexei, H. Miao, O. Yuri, L. Wanshun, and V. Nadezda, About chemical modifications of finite dimensional QED models, *Nonlinear Phenomena in Complex Systems* **24**, 230 (2021).
- [46] H. hui Miao and Y. I. Ozhigov, Using a modified version of the Tavis–Cummings–Hubbard model to simulate the formation of neutral hydrogen molecule, *Physica A: Statistical Mechanics and its Applications* **622**, 128851 (2023).
- [47] H.-h. Miao and Y. I. Ozhigov, Comparing the effects of nuclear and electron spins on the formation of neutral hydrogen molecule, *Lobachevskii Journal of Mathematics* **44**, 3111 (2023).
- [48] H. hui Miao and Y. I. Ozhigov, Distributed computing quantum unitary evolution (2024), arXiv:2403.06937 [quant-ph].
- [49] W. Li, H. hui Miao, and Y. I. Ozhigov, Supercomputer model of finite-dimensional quantum electrodynamics applications (2024), arXiv:2403.07042 [physics.comp-ph].
- [50] W. Pauli, Über den Zusammenhang des Abschlusses der Elektronengruppen im Atom mit der Komplexstruktur der Spektren, *Zeitschrift für Physik* **31**, 765 (1925).
- [51] C. Moler and C. Van Loan, Nineteen dubious ways to compute the exponential of a matrix, *SIAM Review* **20**, 801 (1978).
- [52] C. Moler and C. Van Loan, Nineteen dubious ways to compute the exponential of a matrix, twenty-five years later, *SIAM Review* **45**, 3 (2003).
- [53] W.-x. Zhong and Z.-s. Yang, On the computation of the main eigen-pairs of the continuous-time linear quadratic control problem, *Applied Mathematics and Mechanics* **12**, 45 (1991).
- [54] Z. W X and W. F W, A precise time step integration method, *Proceedings of the Institution of Mechanical Engineers, Part C: Journal of Mechanical Engineering Science* **208**, 427 (1994).
- [55] W.-x. Zhong, On precise time-integration method for structural dynamics, *Journal of Dalian University of Technology* **34**, 131 (1994).
- [56] W.-x. Zhong, Precise integration for transient analysis, *Computational Structure Mechanics and Applications* **12**, 1 (1995).
- [57] G. Qiang, T. ShuJun, and Z. WanXie, A survey of the precise integration method, *SCIENTIA SINICA Technologica* **46**, 1207 (2016).
- [58] A.-S. F. Obada, H. A. Hessian, and A.-B. A. Mohamed, Entropies and entanglement for decoherence without energy relaxation in a two-level atom, *Journal of Physics B: Atomic, Molecular and Optical Physics* **40**, 2241 (2007).

- [59] A.-S. Obada, H. Hessian, and A.-B. Mohamed, Effect of phase-damped cavity on dynamics of tangles of a nondegenerate two-photon JC model, *Optics Communications* **281**, 5189 (2008).
- [60] C. H. Bennett, H. J. Bernstein, S. Popescu, and B. Schumacher, Concentrating partial entanglement by local operations, *Phys. Rev. A* **53**, 2046 (1996).
- [61] Y. Wu and X. Yang, Strong-coupling theory of periodically driven two-level systems, *Phys. Rev. Lett.* **98**, 013601 (2007).